International Journal of Heat and Mass Transfer 115 (2017) 1173–1181

Contents lists available at ScienceDirect

International Journal of Heat and Mass Transfer

journal homepage: www.elsevier.com/locate/ijhmt

Buoyancy effects on heat transfer to supercritical pressure hydrocarbon fuel in a horizontal miniature tube

Jie Wen [a], Haoran Huang [a], Zhouxia Jia [b], Yanchen Fu [a,*], Guoqiang Xu [a]

[a] National Key Laboratory of Science and Technology on Aero-Engine Aero-thermodynamics, Collaborative Innovation Center of Advanced Aero-Engine, School of Energy and Power Engineering, Beihang University, Beijing 100191, People's Republic of China

[b] Science and Technology on Reliability and Environment Engineering Laboratory, Beijing Institute of Structure &Environment Engineering, Beijing 100076, People's Republic of China

ARTICLE INFO

Article history:
Received 22 June 2017
Received in revised form 6 August 2017
Accepted 30 August 2017
Available online 8 September 2017

Keywords:
Heat transfer
Buoyancy
Horizontal
Supercritical
Hydrocarbon fuel

ABSTRACT

Experimental investigations on heat transfer of supercritical pressure aviation hydrocarbon fuel RP-3 in a horizontal miniature round tube were conducted. The influence of buoyancy on heat transfer of RP-3 was studied. Buoyancy effect is particularly significant in horizontal flows, which leads to non-uniform temperature distributions in cross section of the test section even for the miniature round tube. The buoyancy effects of heat transfer can be well evaluated by the non-dimensional parameter Gr_q/Gr_{th} developed by Petukhov. And this criterion was first tested for the horizontal flow in miniature round tube under supercritical pressure conditions. At last, this paper proposed a correlation of Nusselt number for supercritical pressure aviation fuel in the horizontal tube.

1. Introduction

Industrial processes involving heat transfer of supercritical pressure fluids have been taken considerable attention in the past few decades. These applications include supercritical extraction systems using carbon dioxide as extractant, nuclear reactor using supercritical pressure water cooled reactor, rocket motors using hydrogen as working fluid, etc. Besides, the need for enhanced engine performance will drive future gas turbines to higher gas temperature at turbine inlet. In order to achieve this goal, improved material temperature capability and ameliorated cooling techniques have been a primary focus in this area. For these reasons above, the concept of cooled cooling air (CCA) [1,2] was proposed. The air taken off the compressor exit is cooled as it passes through an air-fuel heat exchanger, and then it is taken back into the bore of turbine to cool the rotor. In the typical aero-engine fuel system, the pressure of aviation fuel is 34–68 atm (3.45–6.89 MPa), which is beyond the critical pressure of fuel. In the fuel cooling process, the immense cooling tasks and limited fuel supply require the heat exchanger fuel temperature approaching and rising beyond the critical point.

Many studies [3–17] have been experimentally and numerically investigated on the heat transfer characteristic of supercritical fluids. For a given supercritical pressure, there is a temperature at which the specific heat capacity has a maximum, and variations in other thermo-physical properties with temperature are highest. This temperature is called pseudo-critical temperature. Due to significant variations of thermo-physical properties near the pseudo-critical temperature, heat transfer characteristics are substantially different from the heat transfer behaviors at subcritical pressures.

Petukhov [11] proposed a non-dimensional criteria to evaluate the buoyancy effects on the heat transfer for horizontal flow based on experimental and theoretical research. When $Gr_q < Gr_{th}$, the buoyancy effects on horizontal flow heat transfer is insignificant. Buoyancy effects may lead to non-uniform local wall temperature distributions in experimental pipes. The majority of the theoretical and experimental research in the past decades were for the vertical flows. Bazargan et al. [12] investigated the buoyancy effect on heat transfer of supercritical water in a horizontal round tube. They found that neglecting buoyancy could cause large discrepancies between the predictions of available empirical correlations and the experimental. Shitman [13] investigated the buoyancy effects of supercritical pressure water in horizontal tubes, and he also proposed the product of Prandtl number and Grashof number as a criterion to evaluate the buoyancy effects. Yu et al. [14] investigated the influence of buoyancy on heat transfer to the water in horizontal tube under supercritical pressure. They used two buoyancy criterions to evaluate the buoyancy effects on heat transfer. Recently, Hooman et al. systemically studied the significant buoyancy effect

* Corresponding author.
E-mail address: yanchenfu@buaa.edu.cn (Y. Fu).

http://dx.doi.org/10.1016/j.ijheatmasstransfer.2017.08.116
0017-9310/

Nomenclature

A	surface area
C_p	isobaric specific heat capacity (kJ/(kg·K))
D	diameter (m)
g	gravitational acceleration (m/s^2)
G	mass flow rate (kg/(m^2·s))
Gr	Grashof number
H	enthalpy (kJ/kg)
h	heat transfer coefficient (W/(m^2·K))
I	electrical current (A)
k	thermal conductivity (W/(m·K))
L	length (m)
Nu	Nusselt number
m	mass flow velocity (g/s)
P	pressure (MPa)
Pr	Prandtl number
Q	heat (W)
q	heat flux (kW/m^2)
$R(T)$	electronic resistivity (Ω·m)
r	radius (m)
T	temperature (K)
Re	Reynolds number
U	voltage (V)

Greek

Φ	heat power (W)
β	thermal diffusivity (m^2/s)
ρ	density (kg/m^3)
η	dynamic viscosity (Pa·s)
ν	kinetic viscosity (m^2/s)
λ	thermal conductivity (W/(m·K))

Subscripts

b	bulk
c	critical
in	inside
out	outside
pc	pseudo-critical
w	wall
x	local position

on turbulent convective heat transfer in different channels using numerical method, like inclined pipes [18], corrugated channels [19], concentric and eccentric annuli [20]. It is observed in their research that heat transfer enhancement and deterioration happen at different structures and Reynolds numbers. And then, the experimental research [21] about buoyancy effect of supercritical refrigerant on heat transfer in plate heat exchangers were conducted. The research indicated various heat transfer characteristics occur at different corrugation angles.

Although much work have been done to find out the mechanism of heat transfer at supercritical pressures, this issue is not quite clear and thorough. Especially, most analytical and experimental research focused on the flow and heat transfer in vertical flows. Due to the paucity of experimental data for horizontal flows, more experimental data with heat transfer in horizontal flows are needed. The effects of buoyancy due to heating and its specific convective heat transfer characteristics should be explored.

2. Experimental system

Fig. 1 shows the experimental system. It includes the preparative system, the measured system and reclaimed system. In preparative system, the fuel in tank 1 is pumped up to 15 MPa by a plunger metering pump (SP6015). The mass flow rate of the primary path fuel was measured using a Coriolis-force flow meter (DMF-1-1, 0.15%). In order to pre-heated the fluid to some level of inlet temperatures of the test section, the pre-pressurized primary path fuel was heated (up to 820 K) by two pre-heaters (20 kW, each).

In the test section, a pressure gage transducer (Model 3051CA4, Rosemount) is used to measure the static pressure at the inlet of the test section. The fuel temperature is measured at the inlet and outlet of the test tube with K-type armored thermocouples, respectively. After testing, the heated fuel was cooled lower than 310 K by water cooled shell-tube heat exchanger, and then the water was imported to the water tank after cooled down by the cooling tower. Fig. 2 shows that the test section is a stainless steel (1Cr18Ni9Ti) round tube with the outside diameter of 2.2 mm and a thickness of 0.17 mm. Ten pairs of K-type thermocouples with an accuracy of 0.3 K were welded onto the top and bottom surface of the test tube. A thermally insulated length of 125 mm preceded the heated length of 550 mm, which was followed by a thermally insulated length of 125 mm as shown in Fig. 3.

The accuracy of the mass flow meter was 0.25%. The pressure gage transducer and the differential pressure transducer were calibrated using a pressure calibrator, and the accuracy of the transducers was found to be 0.2% of the reading. All the thermocouples were calibrated in a constant temperature bath and the measurement accuracy was found to be 0.6%. The experimental system was thought to be steady when the inlet, outlet fuel and outside wall temperatures varied within the band of ±0.2 °C and the system pressure and flow rate fluctuations were within ±0.4%. All data were exported in the form of electric signals and recorded by ADAM-4520 system to the computer.

3. Data reduction

The local heat transfer coefficient (HTC) h_x is defined by

$$h_x = \frac{q_x}{T_{wx,in} - T_{b,x}} \tag{1}$$

where the heat flux q_x is the difference of impressed electrical energy and heat losses, and it was defined by

$$q_x = \frac{I^2 R(T)/[\pi(d_o^2 - d_i^2)/4]}{\pi d_i} - q_{loss,x} \tag{2}$$

R(T) is the electrical resistivity of stainless steel, which was gained by correlating the measured electrical resistivity at various wall temperatures (50-600 °C). The heat loss can be gained heat loss calibration tests. Before the experiments, the tube without fuel were directly heated under various heating power and then the heat loss heat flux were fitted with temperature difference between ambient and tube wall. In this study, the proportion of heat loss is less than 4%, which indicated that the test section was well insulated. The inside wall temperature $T_{wx,in}$ was determined by solving the a 1-Dimension heat conduction equation under the cylindrical coordinate system in the following equation.

$$\frac{k}{r}\frac{d}{dr}\left(r\frac{dT}{dr}\right) + \dot{\varphi} = 0 \tag{3}$$

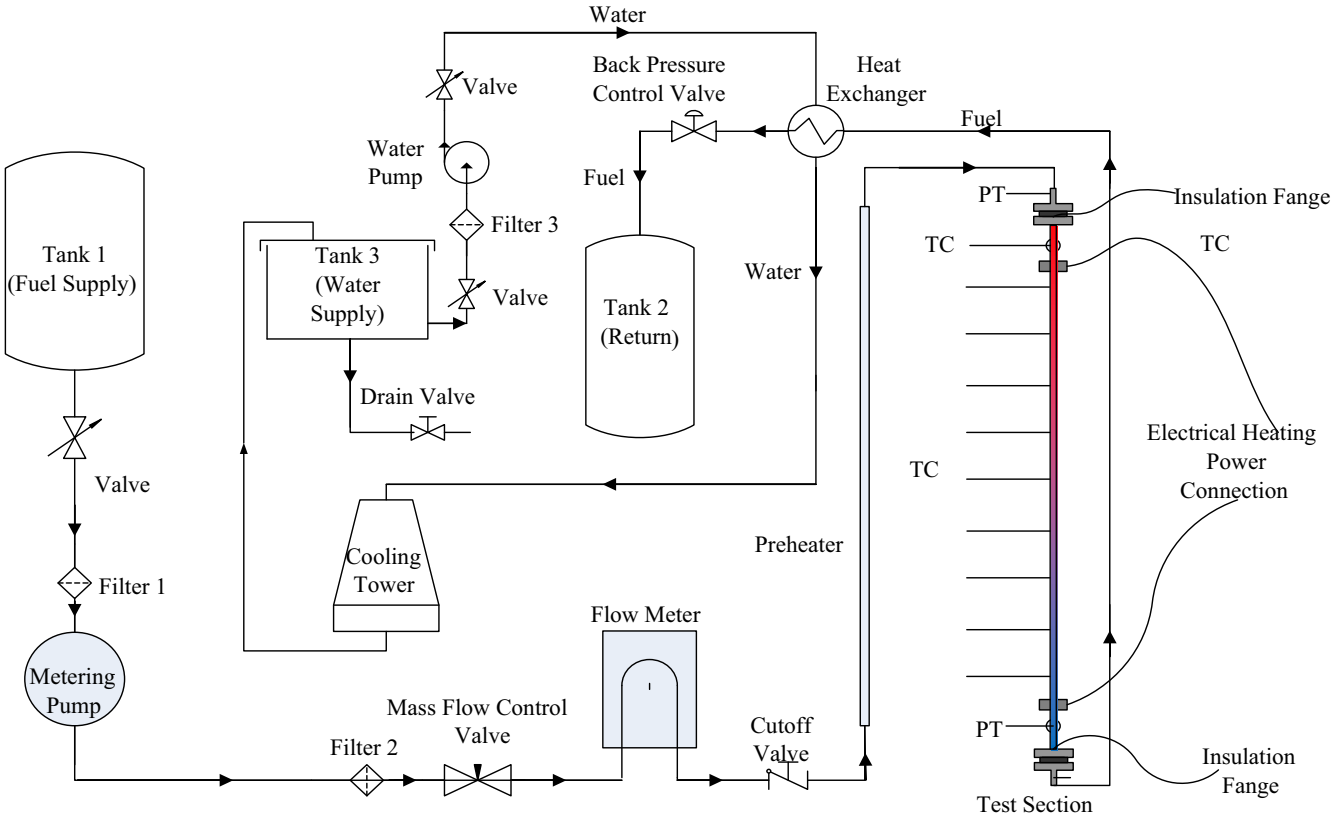

Fig. 1. Schematic of the experimental system.

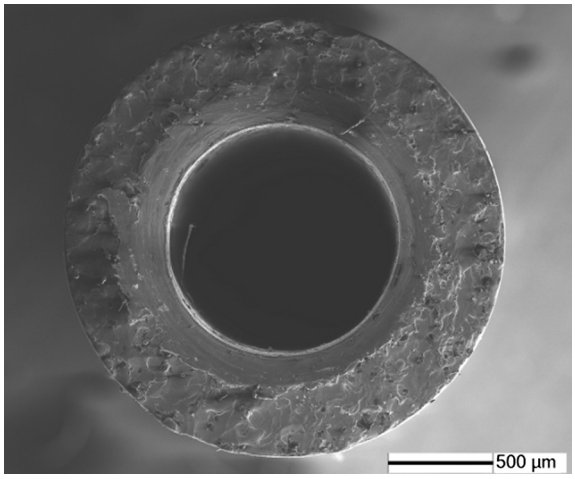

Fig. 2. Cross section of the test tube.

The boundary conditions were

$$q_{loss} = -k\frac{dT}{dr}\Big|_{r=r_{out}} \tag{4}$$

Then $T_{wx,in}$ is given by

$$T_{wx,in} = T_{wx,out} - \left[\left(\dot{\varphi}\frac{r_{out}^2}{2} - q_{x,loss}r_{out}\right)\ln\frac{r_{out}}{r_{in}} - \frac{\dot{\varphi}}{4}\left(r_{out}^2 - r_{in}^2\right)\right]\Big/ k_x \tag{5}$$

The distribution of fuel bulk temperature in the tube can be calculated according to the heating power of the tube wall and the measured RP-3 enthalpy curve [22]. Thus, the fuel bulk temperature is calculated by the inverse function of enthalpy as follows.

$$T_b(x) = H^{-1}\left(H_{b,in} + \frac{q_w(x)\pi d_i x}{m}\right) \tag{6}$$

And then the local Nusselt number is defined by

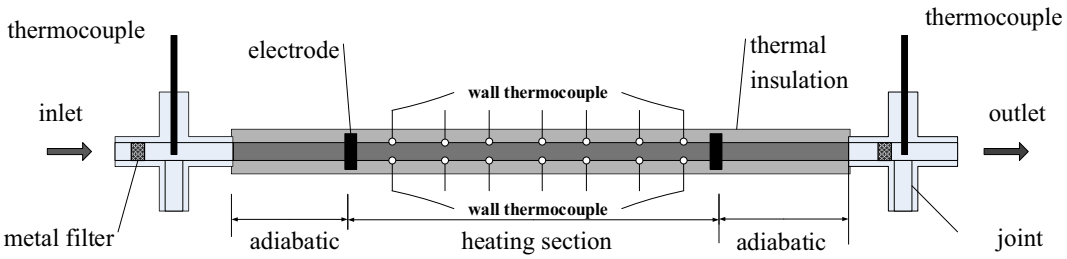

Fig. 3. Schematic of horizontal tube.

$$Nu_x = \frac{h_x d}{\lambda_x} \tag{7}$$

where λ_x is the local thermal conductivity of RP-3. The Reynolds number was defined based on the mean bulk temperature:

$$Re = \frac{\rho u d_i}{\mu} = \frac{4m}{\pi d_i \mu} \tag{8}$$

As thermal properties sharply change with the variation of temperatures, it is important to know when the buoyancy effects are significant and when it is not. The dimensionless buoyancy parameter, Gr_{th} and Gr_q introduced by Petukhov et al. [11] used to evaluate the buoyancy effect was defined as

$$Gr_q = \frac{g\overline{\beta} q'' d^4}{v_b^2 \lambda_b} \tag{9}$$

$$Gr_{th} = 3 \times 10^{-5} Re_b^{2.75} \overline{Pr}^{0.5} [1 + 2.4 Re_b^{-1/8} (\overline{Pr}^{2/3} - 1)] \tag{10}$$

$$\overline{Pr} = \frac{i_w - i_b}{T_w - T_b} \frac{\mu_b}{k_b} \tag{11}$$

$$\overline{\beta} = \frac{1}{\rho_{film}} \frac{\rho_b - \rho_w}{T_w - T_b} \tag{12}$$

where i and T represent the enthalpy and temperature. The subscripts w and b correspond to the wall and bulk temperature. According to the error transfer formula and previous similar uncertainty analysis [23], the effective tube wall heat flux is obtained as follows.

$$\left|\frac{\Delta q_x}{q_x}\right| = \sqrt{\left(\frac{q_{0,x}}{q_x}\right)^2 \varepsilon^2(q_{0,x}) + \left(\frac{q_{loss,x}}{q_x}\right)^2 \varepsilon^2(q_{loss,x})} \tag{13}$$

As the ratio of heat loss heat flux and effective heat flux in the experiment is not more than 5%, the uncertainty of the tube wall heat flux is about 2.7%. In addition, the temperature difference between fluid and inner wall is larger than 35 K. Hence, the following equation is obtained.

$$\left|\frac{\delta(\Delta T)}{\Delta T}\right| = \frac{\sqrt{|\delta T_{wx,in}|^2 + |\delta T_{bx}|^2}}{35} = 3.9\% \tag{14}$$

Combining the uncertainties of heat flux and temperature difference, the local heat transfer coefficient could be calculated as follows:

$$\left|\frac{\Delta h_x}{h_x}\right| = \sqrt{\varepsilon^2(q_x) + \varepsilon^2(\Delta T)} = \sqrt{(2.7\%)^2 + (3.9\%)^2} = 4.7\% \tag{15}$$

According to previous measurement data of hydrocarbon fuel thermal conductivity [24], the measurement uncertainty is no larger than 3%. Thus, the uncertainty of Nusselt number is calculated as follows:

$$\left|\frac{\Delta Nu_x}{Nu_x}\right| = \sqrt{\varepsilon^2(h_x) + \varepsilon^2(\lambda)} = \sqrt{(4.7\%)^2 + (3.0\%)^2} = 5.6\% \tag{16}$$

For the purpose of validating accuracy and repeatability of the experimental system, validation test was performed using toluene under various conditions. The experimental *Nu* number was compared with the data calculated using the Dittus-Boelter equation as shown in Fig. 4. The deviation between experimental data and calculated ones is within an error band of ±6%, which indicates that the experimental rig is reliable and convincing.

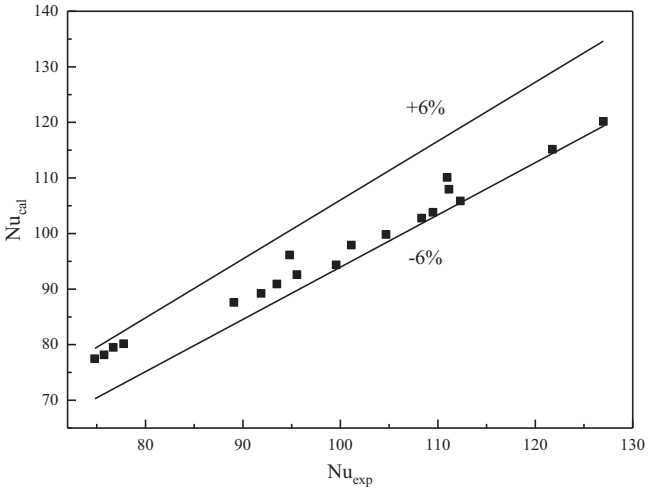

Fig. 4. Validation of the experimental system.

4. Material

A typical aviation kerosene RP-3, which is the most popular jet fuel used in the aero engines in China, is used in this work. Composition analysis by using GC6890-MS5975 shows that RP-3 consists of 52.44% alkanes, 7.64% alkenes, 18.53% benzenes, 15.54% cycloalkanes, 4.39% naphthalenes and 1.46% other compositions, the detailed compositions of RP-3 are listed in Deng's work [25]. The critical point of RP-3 was identified as (T_c = 645.04 K, P_c = 2.34 MPa) [26] due to the most obvious critical opalescence phenomenon conducted in our previous work. The thermophysical and transport properties of kerosene RP-3 were measured in our previous work [24,25,27,28] as shown in Fig. 5. Besides, Toluene used in the validation tests is purified with a purity of 99.9%.

The pseudo-critical temperatures were determined by the specific heat capacity measurements at several supercritical pressures [27]. According to these experimental data, the relationship between pseudo-critical temperatures and pressures is expressed as equation below using polynomial fitting with the average error of 0.38%.

$$T_{pc} = -1.78 \times p^3 + 13.24 \times p^2 + 4.48 \times p + 585.2 \tag{17}$$

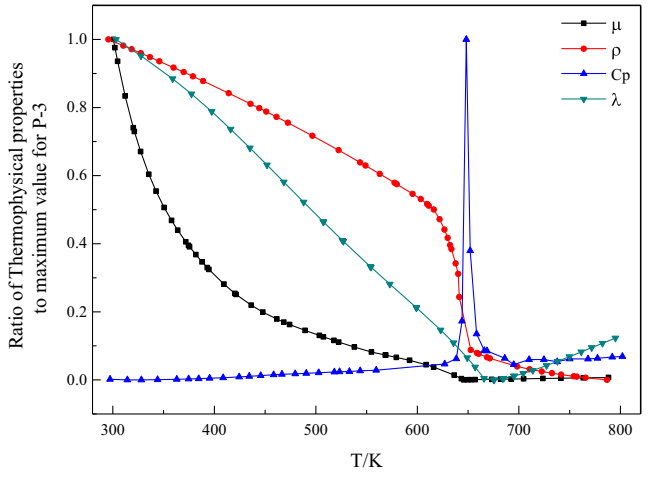

Fig. 5. Thermo-physical properties variations of RP-3 with temperature.

5. Results and discussion

The heat transfer of supercritical pressure kerosene RP-3 flowing through a 1.86 mm inner diameter horizontal tube was investigated for inlet pressure of 3–5 MPa which is beyond the critical pressure 2.33 MPa. The distributions of the local wall temperature, HTC and buoyancy number Gr_q/Gr_{th} are presented for various wall heat fluxes, system pressures, inlet temperatures and Reynolds numbers.

5.1. Effect of heat flux

Figs. 6a and 6b shows inner wall mean, fluid temperatures and HTC variations along the tube under different heat fluxes when the system pressure, inlet temperature and mass flow rate are fixed at 5 MPa, 473 K and 736 kg/m^2 s. At the beginning of the test tube, the HTC decreases with the increase of the heat flux and then comes to the same level. When the dimensionless position x/d is larger than 110, higher heat flux induces the larger heat transfer ability for various conditions. This is explained by the fact that there exists large wall temperature gradient near the wall at the inlet region and buoyancy effect weakens the shear force to make the flow laminarization. Besides, this kind of heat transfer deterioration enhances with the increase of heat flux. With the flow developing and temperature rising, the increase of heat capacity and decrease of viscosity as displayed in Fig. 5 strength the convective heat transfer.

In horizontal flows, buoyancy effects may result in the non-uniform temperature distributions at the cross-section of tube. To be specific, buoyancy effects make the hotter fluid go up to the top surface and the colder fluid go down to the bottom surface of the tube. Therefore, the heat transfer capacity at top surface is worse than that at bottom surface. So the temperature difference between top and bottom surfaces of the test tube can be regarded as a measure of buoyancy effects. For the small diameter (1.86 mm) round tube, the temperature difference between top and bottom surfaces of the test tube can be 50 K for some conditions, which was barely reported in previous research. A wall temperature peak and trough were measured at both top and bottom surface of the test tube as the fluid bulk enthalpy increases (373–840 K) as shown in Fig. 7a. The x-axis in the figure represents the enthalpy at different temperatures and the two lines represent the pseudo-critical temperature and its bulk enthalpy. It is obvious that heat transfer was enhanced significantly near the pseudo-critical temperature region due to sharp increase of isobaric

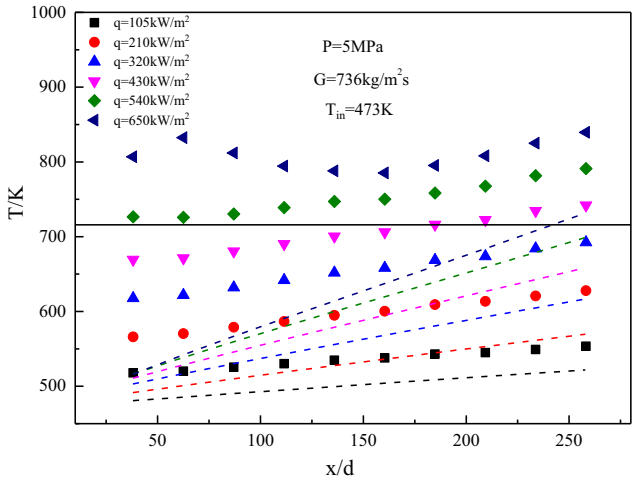

Fig. 6a. Inner wall mean and fluid temperatures variations at different heat fluxes.

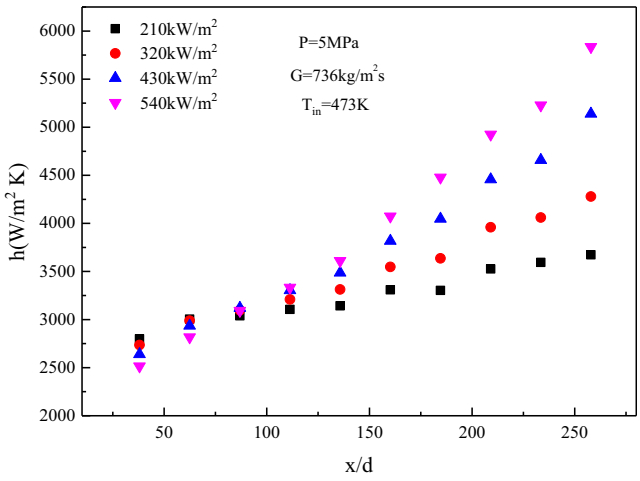

Fig. 6b. HTC variations at different heat fluxes.

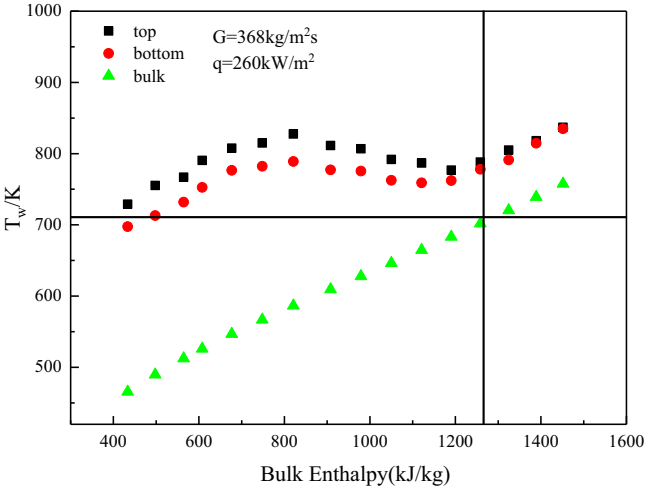

Fig. 7a. Top and bottom wall temperature variations with bulk enthalpy.

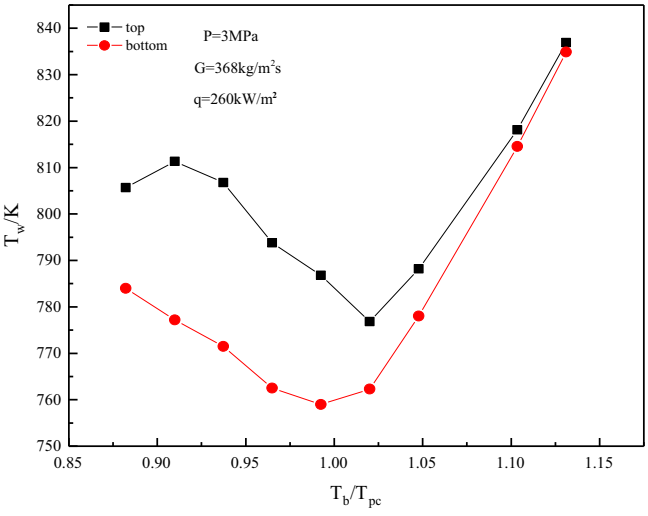

Fig. 7b. Temperature variations between top and bottom surface of test tube with dimensionless bulk temperature.

specific heat capacity. And the temperature difference between top and bottom surface of the test tube decrease dramatically at the same region.

Fig. 7b shows wall temperature at top and bottom surface of test tube variations with non-dimensional fluid bulk temperature. It can be seen that as the bulk temperature exceeds the pseudo-critical temperature at the supercritical pressure, the temperature difference between top and bottom surface decreases. For heat transfer in horizontal flow, large density gradient produces significant buoyancy effects. For explanation, as fluid bulk temperature approaches the pseudo-critical temperature, heat transfer was enhanced obviously due to sharp increase of specific isobaric heat capacity between the wall and fluid. The slope of density variations with temperature is greater prior to pseudo-critical temperature. As a result, larger density gradient in radial direction make the buoyancy effects significant before the pseudo-critical temperature.

The wall temperature distributions of top and bottom surface of the test tube at various heat fluxes under 3 MPa pressure and 368 kg/ (m^2s) mass flow rate are shown in Fig. 8a. The temperature difference between top and bottom surface is very small at low heat flux, showing insignificant buoyancy effects. And then with higher heat fluxes of 210 kW/m^2 and 320 kW/m^2, the buoyancy effects become significant leading to higher temperature difference between top and bottom surface when the dimensionless position x/d does not exceed 180. Specially, a temperature peak exists in the entrance section at both top and bottom of the test tube. These phenomena could be matched with the buoyancy factor Gr_q/Gr_{th} variations along the tubes as shown in Fig. 8b. At higher heat flux conditions, the value of Gr_q/Gr_{th} is larger than 1 when the dimensionless position x/d < 180 and significant temperature difference appears. This can be also explained by the fact that the thinner thermal boundary layer due to the entrance effects enhances the heat transfer at the initial part of the test tube.

5.2. Effect of mass flow rate

As the system pressure, inlet temperature and heat flux are fixed, different mass flow rate could lead to various inlet Reynolds number and flow status. Figs. 9a and 9b show variations of inner wall mean temperature and HTC under inlet Reynolds number from 3760 to 11340. It is demonstrated that inner wall temperatures along the tube are much larger than the pseudo-critical temperature (669.8 K) at 3 MPa system pressure when the inlet

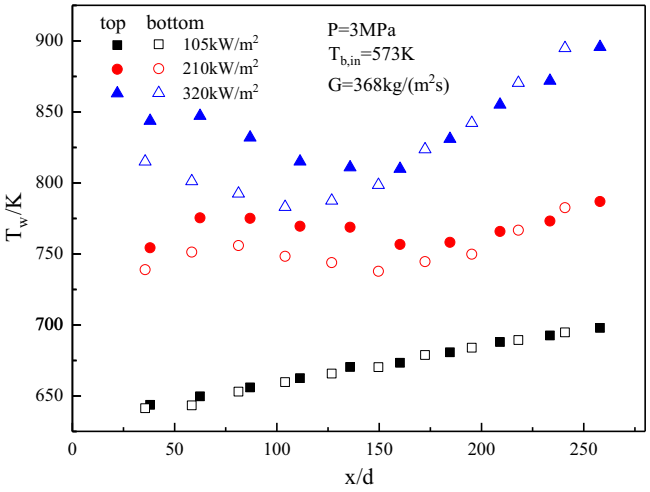

Fig. 8a. Wall temperature distributions along the tube at various heat fluxes.

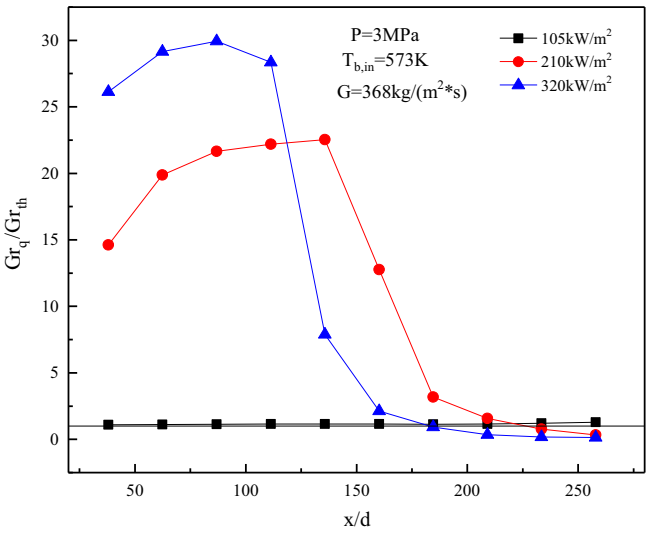

Fig. 8b. Gr_q/Gr_{th} distributions along the tube at various heat fluxes.

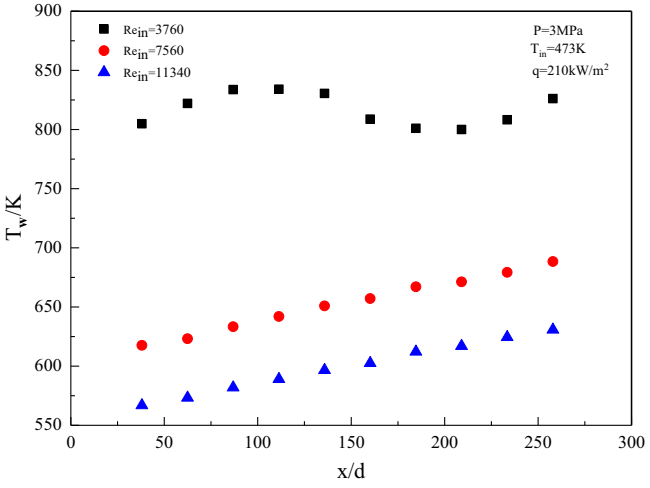

Fig. 9a. Inner wall mean temperatures variations at different mass flow rates.

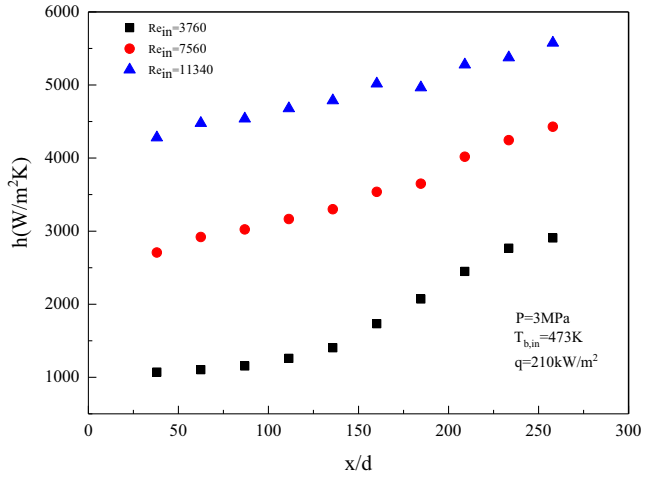

Fig. 9b. HTC variations at different mass flow rates.

Reynolds number is 3760. The buoyancy induced by the temperature difference between the bulk and the near wall inhibits the increase of HTC and increases the inner wall temperature. And then the bulk temperature rise leads to the enhancement of turbulent kinetic energy and weakens the buoyancy effect. Thus, the heat transfer recovers to the normal status and the inner wall temperature peak happens at the dimensionless position x/d = 125. With the inlet Reynolds number increasing, the turbulent kinetic energy simultaneously increases along the test tube and the buoyancy effect could be neglected. Therefore, the heat transfer characteristics belong to the normal status when the inlet Reynolds numbers are 7560 and 11340.

Figs. 10a and 10b shows the temperature distributions at top and bottom surface of the test tube and Gr_q/Gr_{th} distributions at various mass flow rates. As the mass flow rate decreases, the temperature difference between top and bottom surface of the test tube increases, which shows weakened buoyancy effects. For explanation, more turbulence energy produced by higher mass flow rate suppresses buoyancy effects. To be specific, Gr_q/Gr_{th} is much higher for low mass flow rate condition before the location of x/d = 230 and then the ratio drops to near unity, which is in accordance with the buoyancy effects on heat transfer as shown in Fig. 10a. The wall temperatures at both top and bottom surface show a peak and a valley at different positions along the tube. It is explained that the entrance effects could induce the thicker thermal boundary layer, and then specific heat capacity increase and viscosity decrease enhance heat transfer capacity at higher fluid temperatures.

5.3. Effect of system pressure

Fig. 11a shows Gr_q/Gr_{th} variations along with dimensionless fluid bulk temperature under different system pressures. It is indicated that the ratio firstly increases to the peak value and sharply decreases to the value 1 at the region near the pseudo-critical point. During this process, the maximum value could achieve at about 35, which shows strong buoyancy effect at the contrast temperature T_b/T_{pc} = 0.9. This variation could match the principle of buoyancy effect on the convective heat transfer and the significant effect is reflected by the temperature difference between the top and bottom surfaces of the test tube. Furthermore, the ratio at 5 MPa pressure is lower than that at 3 MPa for the same bulk temperature, and this illustrates that the improvement of system

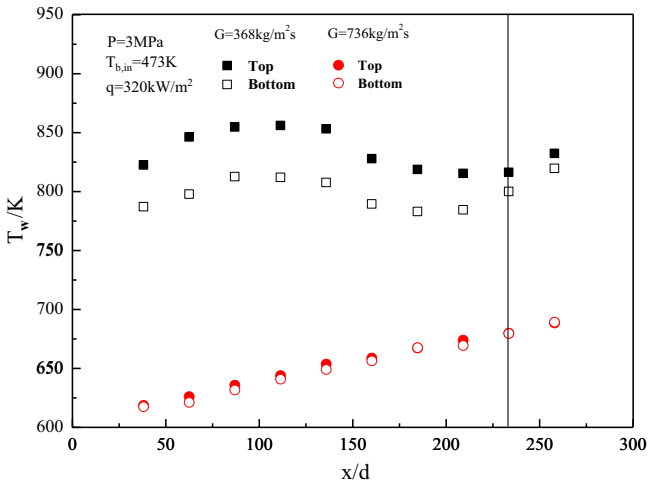

Fig. 10a. Top and bottom wall temperature distribution along the tube at various mass flow rate.

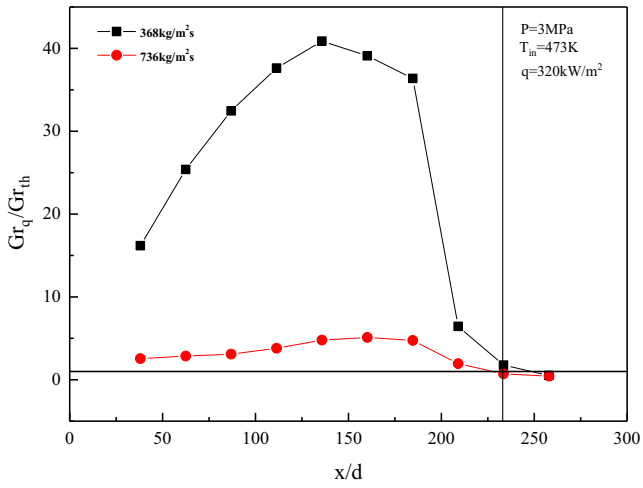

Fig. 10b. Gr_q/Gr_{th} distribution along the tube at various mass flow rate.

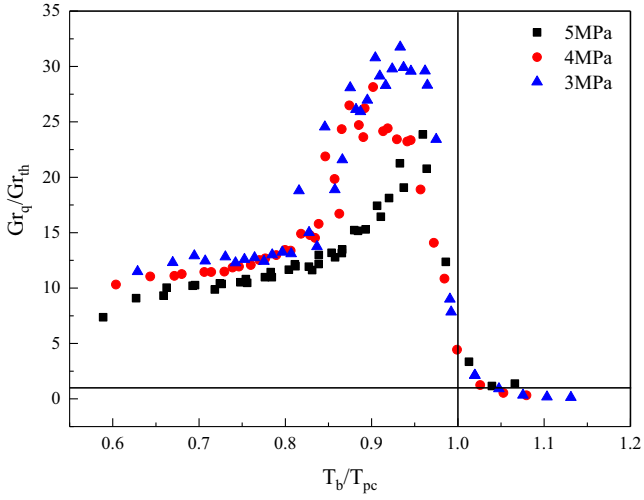

Fig. 11a. Gr_q/Gr_{th} variations with dimensionless bulk temperature at various system pressures.

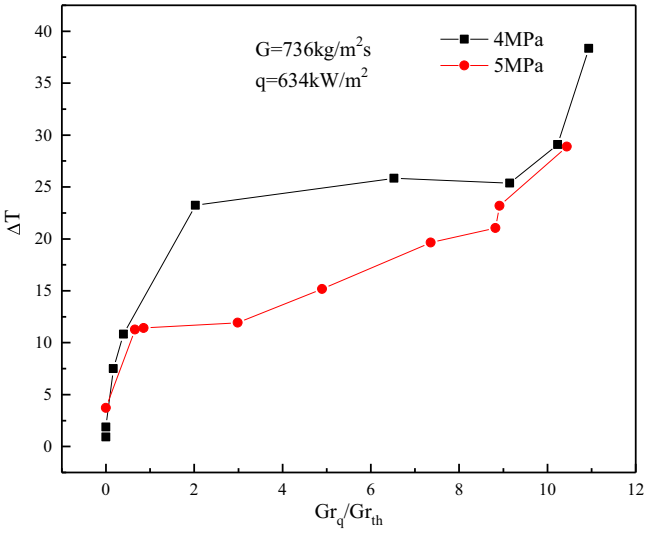

Fig. 11b. ΔT variations with Gr_q/Gr_{th} at various system pressures.

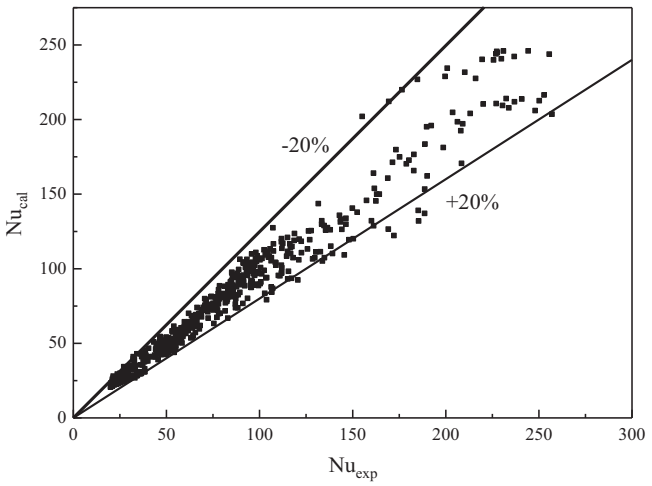

Fig. 12. Deviations between calculated *Nu* number and experimental values.

pressure could strain the buoyancy effect on horizontal convective heat transfer.

Fig. 11b shows the temperature difference variations between top and bottom surface of test tube along with dimensionless Gr_q/Gr_{th} at various pressures. It is obvious that with greater temperature difference between top and bottom surface of the test tube, the magnitude of Gr_q/Gr_{th} is greater in all experimental cases. When the Gr_q/Gr_{th} is larger than 1, the temperature difference is averagely larger than 10 and the maximum value could reach about 40 K. Therefore, buoyancy effects on heat transfer in horizontal flow can be well evaluated by this dimensionless Gr_q/Gr_{th}.

5.4. Heat transfer correlation

Based on the experimental data, a correlation of Nusselt number for supercritical pressure aviation fuel in horizontal tube was proposed as shown in Eq. (18). The correlation was modified using the multiple linear regression method according to the Dittus-Boelter equation considering the thermal physical properties correction. Also, the wall temperatures are adopted by the mean temperature between top and bottom surface temperatures. Fig. 12 shows the deviation between calculated values of Nusselt number and experimental ones.

$$Nu = 0.001367 Re^{1.097} Pr^{0.36} \left(\frac{\rho_w}{\rho_b}\right)^{0.154} \left(\frac{c_{p,m}}{c_{p,b}}\right)^{0.6} \quad (18)$$

Where subscript b stands for the fluid bulk temperature, and m indicates that the thermo-physical properties are based on the average value in the boundary layer. The mean temperature isobaric heat capacity could be calculated by the following equation.

$$c_{p,m} = \frac{H_w - H_b}{T_w - T_b} \quad (19)$$

H_w and H_b represent the enthalpy at the wall and bulk temperatures, respectively.

As show in Fig. 12, the average deviation between calculated Nusselt number and experimental ones is 11.3%, and the majority (84.4%) of deviation between the calculated Nusselt and the experimental ones are in the error band of 20%.

6. Conclusion

This paper studies the heat transfer characteristics and buoyancy effects on heat transfer of supercritical pressure hydrocarbon fuel in horizontal flow. The main characteristics of supercritical pressure fluids is the large buoyancy effects. Heat transfer impairment occurs in the initial part of test tube due to entrance effects. Buoyancy effect is particularly significant in horizontal flows, which leads to non-uniform temperature distributions at the cross section of test section, even for the miniature round tube. And this heat transfer impairment is more obvious at higher heat flux conditions. Higher mass flow rate and lower heat flux can suppress buoyancy effects on heat transfer. The buoyancy effects of heat transfer could be well evaluated by the non-dimensional parameter Gr_q/Gr_{th} developed by Petukhov. And this criterion was first tested for horizontal flow in the miniature round tube. Furthermore, a correlation of Nusselt number for supercritical pressure hydrocarbon fuel in a horizontal tube was proposed.

Conflict of interest

The authors declared that they have no conflicts of interest to this work.

References

[1] G. Bruening, W. Chang, Cooled cooling air systems for turbine thermal management, ASME Paper (99-GT) (1999) 14.
[2] H. Huang, L.J. Spadaccini, D.R. Sobel, Fuel-cooled thermal management for advanced aeroengines, J. Eng. Gas Turb. Power 126 (2) (2004) 284.
[3] J. Jackson, Some striking features of heat transfer with fluids at pressures and temperatures near the critical point, in: Keynote Paper for International Conference on Energy Conversion and Application (ICECA 2001), Wuhan, China, 2001.
[4] J. Jackson, W. Hall, Influences of buoyancy on heat transfer to fluids flowing in vertical tubes under turbulent conditions, Turbulent forced convection in channels and bundles 2 (1979) 613–640.
[5] S. Liao, T. Zhao, An experimental investigation of convection heat transfer to supercritical carbon dioxide in miniature tubes, Int. J. Heat Mass Transf. 45 (25) (2002) 5025–5034.
[6] P.-X. Jiang, Y. Zhang, Y.-J. Xu, R.-F. Shi, Experimental and numerical investigation of convection heat transfer of CO_2 at supercritical pressures in a vertical tube at low Reynolds numbers, Int. J. Therm. Sci. 47 (8) (2008) 998–1011.
[7] P.-X. Jiang, B. Liu, C.-R. Zhao, F. Luo, Convection heat transfer of supercritical pressure carbon dioxide in a vertical micro tube from transition to turbulent flow regime, Int. J. Heat Mass Transf. 56 (1) (2013) 741–749.
[8] J. Jackson, M. Cotton, B. Axcell, Studies of mixed convection in vertical tubes, Int. J. Hat Fluid Fl. 10 (1) (1989) 2–15.
[9] G. Kuang, M. Ohadi, Y. Zhao, Experimental study on gas cooling heat transfer for supercritical CO2 in microchannels, in: ASME 2004 2nd International Conference on Microchannels and Minichannels, American Society of Mechanical Engineers, 2004, pp. 325–332.
[10] J. Jackson, W. Hall, Forced convection heat transfer to fluids at supercritical pressure, Turbulent forced convection in channels and bundles 2 (1979) 563–611.
[11] B. Petukhov, A. Polyakof, V. Kuleshov, Y.L. Sheckter, Turbulent flow and heat transfer in horizontal tubes with substantial influence of thermo-gravitational forces, in: Proc. of Fifth Int. Heat Transfer Conference, 1974, pp. 3–7.
[12] M. Bazargan, D. Fraser, V. Chatoorgan, Effect of buoyancy on heat transfer in supercritical water flow in a horizontal round Tube, J. Heat Trans-T. ASME 127 (8) (2005) 897.
[13] M. Shitsman, The effect of natural convection on temperature conditions in horizontal tubes at supercritical pressures, Therm. Eng 13 (7) (1966) 69–75.
[14] S. Yu, H. Li, X. Lei, Y. Feng, Y. Zhang, H. He, T. Wang, Influence of buoyancy on heat transfer to water flowing in horizontal tubes under supercritical pressure, App. Therm. Eng. 59 (1–2) (2013) 380–388.
[15] M. Watts, C. Chou, Mixed convection heat transfer to supercritical pressure water, in: Proceedings of the 7th International Heat Transfer Conference, 1982, pp. 495–500.
[16] J.D. Jackson, Fluid flow and convective heat transfer to fluids at supercritical pressure, Nucl. Eng. Des. 264 (2013) 24–40.
[17] I.L. Pioro, R.B. Duffey, Experimental heat transfer in supercritical water flowing inside channels (survey), Nucl. Eng. Des. 235 (22) (2005) 2407–2430.
[18] P. Forooghi, K. Hooman, Numerical study of turbulent convection in inclined pipes with significant buoyancy influence, Int. J. Heat Mass Transf. 61 (2013) 310–322.
[19] P. Forooghi, K. Hooman, Effect of buoyancy on turbulent convection heat transfer in corrugated channels–a numerical study, Int. J. Heat Mass Transf. 64 (2013) 850–862.
[20] P. Forooghi, I.A. Abdi, M. Dahari, K. Hooman, Buoyancy induced heat transfer deterioration in vertical concentric and eccentric annuli, Int. J. Heat Mass Transf. 81 (2015) 222–233.

[21] P. Forooghi, K. Hooman, Experimental analysis of heat transfer of supercritical fluids in plate heat exchangers, Int. J. Heat Mass Transf. 74 (2014) 448–459.
[22] C. Zhang, H. Deng, G. Xu, W. Huang, K. Zhu, Enthalpy measurement and heat transfer investigation of RP-3 kerosene at supercritical pressure, J. Aerosp. Power 25 (2) (2010) 331–335.
[23] Y. Fu, H. Huang, J. Wen, G. Xu, W. Zhao, Experimental investigation on convective heat transfer of supercritical RP-3 in vertical miniature tubes with various diameters, Int. J. Heat Mass Transf. 112 (2017) 814–824.
[24] G. Xu, Z. Jia, J. Wen, H. Deng, Y. Fu, Thermal-conductivity measurements of aviation kerosene RP-3 from (285 to 513) K at sub-and supercritical pressures, Int. J. Thermophys. 36 (4) (2015) 620–632.
[25] H. Deng, C. Zhang, G. Xu, Z. Tao, B. Zhang, G. Liu, Density measurements of endothermic hydrocarbon fuel at sub-and supercritical conditions, J. Chem. Eng. Data 56 (6) (2011) 2980–2986.
[26] H. Deng, C. Zhang, G. Xu, Z. Tao, K. Zhu, Y. Wang, Visualization Experiments of a Specific Fuel Flow Through Quartz-glass Tubes Under both Sub- and Supercritical Conditions, Chinese J. Aeronaut. 25 (3) (2012) 372–380.
[27] H. Deng, K. Zhu, G. Xu, Z. Tao, C. Zhang, G. Liu, Isobaric specific heat capacity measurement for kerosene RP-3 in the near-critical and supercritical regions, J. Chem. Eng. Data 57 (2) (2011) 263–268.
[28] H. Deng, C. Zhang, G. Xu, B. Zhang, Z. Tao, K. Zhu, Viscosity measurements of endothermic hydrocarbon fuel from (298 to 788) K under supercritical pressure conditions, J. Chem. Eng. Data 57 (2) (2012) 358–365.